Monthly Notices of the ROYAL ASTRONOMICAL SOCIETY

MNRAS **530,** L1–L6 (2024)
Advance Access publication 2024 February 29

https://doi.org/10.1093/mnrasl/slae017

Synchrotron signatures of cosmic ray transport physics in galaxies

Sam B. Ponnada [1]★ Iryna S. Butsky [1,2] Raphael Skalidis [1] Philip F. Hopkins [1] Georgia V. Panopoulou [3] Cameron Hummels,[1] Dušan Kereš,[4] Eliot Quataert [5] Claude-André Faucher-Giguère [6] and Kung-Yi Su[7]

[1]*California Institute of Technology, TAPIR, Mailcode 350-17, Pasadena, CA 91125, USA*
[2]*Kavli Institute for Particle Astrophysics and Cosmology (KIPAC), Stanford University, Stanford, CA 94305, USA*
[3]*Department of Space, Earth and Environment, Chalmers University of Technology, SE-412 93, Göteborg, Sweden*
[4]*Department of Physics, Center for Astrophysics and Space Sciences, University of California San Diego, 9500 Gilman Drive, La Jolla, CA 92093, USA*
[5]*Department of Astrophysical Sciences, Princeton University, Princeton, NJ 08544, USA*
[6]*Department of Physics and Astronomy and CIERA, Northwestern University, 2145 Sheridan Road, Evanston, IL 60208, USA*
[7]*Black Hole Initiative, Harvard University, 20 Garden Street, Cambridge, MA 02138, USA*

Accepted 2024 February 28. Received 2024 February 21; in original form 2023 September 28

ABSTRACT

Cosmic rays (CRs) may drive outflows and alter the phase structure of the circumgalactic medium, with potentially important implications on galaxy formation. However, these effects ultimately depend on the dominant mode of transport of CRs within and around galaxies, which remains highly uncertain. To explore potential observable constraints on CR transport, we investigate a set of cosmological FIRE-2 CR-magnetohydrodynamic simulations of L_* galaxies which evolve CRs with transport models motivated by self-confinement (SC) and extrinsic turbulence (ET) paradigms. To first order, the synchrotron properties diverge between SC and ET models due to a CR physics-driven hysteresis. SC models show a higher tendency to undergo 'ejective' feedback events due to a runaway buildup of CR pressure in dense gas due to the behaviour of SC transport scalings at extremal CR energy densities. The corresponding CR wind-driven hysteresis results in brighter, smoother, and more extended synchrotron emission in SC runs relative to ET and constant diffusion runs. The differences in synchrotron arise from different morphology, interstellar medium gas, and **B** properties, potentially ruling out SC as the dominant mode of CR transport in typical star-forming L_* galaxies, and indicating the prospect for non-thermal radio continuum observations to constrain CR transport physics.

Key words: methods: numerical – cosmic rays – ISM: magnetic fields – galaxies: formation.

1 INTRODUCTION

Relativistic charged particles, or cosmic rays (CRs), are ubiquitous in the Universe. Injected and accelerated at supernovae (SNe), stellar winds, and associated shocks fronts, CRs are known to be a considerable component of the Milky Way (MW) interstellar medium (ISM, Bell 1978; Boulares & Cox 1990) and are observed in other L_* galaxies via their γ-ray and non-thermal synchrotron radiation (Lacki et al. 2011; Tang, Wang & Tam 2014).

In the past decade, the importance of CRs as a source of feedback in galaxies has come to be appreciated (for recent reviews, see Owen et al. 2023; Ruszkowski & Pfrommer 2023). A host of theoretical studies employing varied numerical and physical prescriptions have established that CRs can play an important role in driving and altering the structure of winds (Booth et al. 2013; Salem & Bryan 2014; Girichidis et al. 2016; Pakmor et al. 2016; Simpson et al. 2016; Bustard et al. 2020; Armillotta, Ostriker & Jiang 2022; Huang & Davis 2022; Huang, Jiang & Davis 2022; Quataert, Thompson & Jiang 2022; Modak et al. 2023; Thomas, Pfrommer & Pakmor 2023) and providing a potentially key source of non-thermal pressure support in the circumgalactic medium (CGM, Butsky & Quinn 2018; Chan et al. 2019; Buck et al. 2020; Hopkins et al. 2020; Farcy et al. 2022).

These effects can manifestly change the star formation histories of L_* galaxies by preventing cool gas from precipitating onto the disc, altering the dynamics of gas in the tenuous inner CGM (Butsky et al. 2022) or 'disc–halo interface'(Chan et al. 2021) with potential implications on the amplification of magnetic fields (Ponnada et al. 2022) as well as the phase structure and ionization state of halo gas (Salem, Bryan & Corlies 2016; Butsky et al. 2020; Ji et al. 2020; Tsung, Oh & Bustard 2023).

However, a major caveat remains that all of the aforementioned effects depend sensitively on the dominant mode of transport of CRs through the ISM and into the CGM, which is highly uncertain with elusive observational constraints (Hopkins et al. 2021a). An understanding of CR transport is thus crucial to contextualize the importance of CRs for galaxy formation and evolution, as CR effects in the ISM and CGM are heavily dependent on the macroscopic transport speed, often parametrized through the diffusion coefficient κ (more specifically, $\kappa_\parallel$), or streaming speed $v_{\rm st}$.

The transport of CRs on ∼kpc–Mpc galactic scales is fundamentally tied to the scattering of CRs on orders of magnitude smaller gyro-resonant scales (∼ 0.1 au for ∼GeV CRs). Thus, there has been

★ E-mail: sponnada@caltech.edu

increasing theoretical interest in understanding the macro-physical transport properties of CRs motivated by models of plasma-scale CR transport (Jokipii 1966; Skilling 1975) and how their predicted observables compare to observations (Hopkins et al. 2021b, 2022; Kempski & Quataert 2022; Butsky et al. 2023).

Despite some constraining power of existing observations, there is a dire need for further observational comparison to narrow the broad theoretical parameter space, which radio-continuum synchrotron observations may provide. In this letter, we forward-model synchrotron emission from cosmological, zoom-in simulations of galaxy formation including CRs with different physically motivated CR transport models from the Feedback in Realistic Environments (FIRE) suite[1] (Hopkins et al. 2018, 2021b) and explore the physical basis for corresponding observable differences which emerge owing to CR physics. In Section 2, we briefly describe the simulations and our methods. Then, we present our results for models with varied CR transport physics in Section 3. Lastly, we discuss our conclusions in Section 4.

2 SIMULATIONS AND METHODS

In this study, we utilize a subset of the simulations presented in Hopkins et al. (2021a, b) which evolve a 'single-bin' of 1–10 GeV CRs and utilize FIRE-2 (Hopkins et al. 2018) physics. We summarize the most pertinent aspects here, but refer the reader to the aforementioned papers for a more in-depth discussion of numerical details.

The simulations are all fully cosmological, magnetohydrodynamic (MHD, Hopkins 2016; Hopkins & Raives 2016) simulations of galaxy formation which include baryons and dark matter, fully anisotropic Spitzer–Braginskii conduction and viscosity (Hopkins 2017) at a Lagrangian mass resolution of 56 000 $M_\odot$. Prescriptions for explicit stellar feedback and gas cooling (for $T \sim 10$–10^{10} K) follow (Hopkins et al. 2018); stars form in dense ($n > 1000$ cm^{-3}), self-shielded, Jeans unstable gas with multiband radiation, mass-loss, and explosive feedback from Types Ia and II SNe (evolved self-consistently following stellar evolution models) coupled to gas.

CRs are injected from SNe and OB/WR stellar winds with an energy efficiency of $\epsilon_{\rm CR} = 0.1$ of the initial ejecta kinetic energy. In these 'single-bin' simulations, we solely evolve the ∼1–10 GeV CR energy density ($e_{\rm CR}$), or equivalently a constant spectral distribution, as a relativistic fluid with $\gamma_{\rm CR} = 4/3$. The CR dynamics are coupled to the gas and evolve self-consistently, with transport coupled to magnetic field lines according to the CR transport equations and loss terms (collisional and streaming) computed in-code (again, see details in Hopkins et al. 2021b).

These simulations invoke scalings for the CR scattering rate, ν, with various plasma properties motivated by microphysical scenarios. One such model class includes 'extrinsic turbulence' (ET) scenarios (Jokipii 1966), where CRs are scattered off of gyro-resonant fluctuations in **B** on scales of order the CR gyro radius that arise from a turbulent cascade down to those (small) scales. Model variants in this general class vary widely (as shown in Hopkins et al. 2021b) according to uncertainties in the shape of the turbulent cascade at small scales, which turbulent modes are of primary importance for scattering on these scales, the importance of certain damping terms, and geometric considerations of the (an)isotropy of said turbulent modes. But broadly speaking, the assumption for our purposes is that the scattering rate ν varies with the local Alfvén scale ($\ell_{\rm A}$) and Alfv´en Mach number ($\mathcal{M}_{\rm A}$) of turbulence on *resolved* simulation scales as $\nu \propto \mathcal{M}_{\rm A}^2/\ell_{\rm A}$. The normalization of ν for these models at ∼1 GeV is fitted by Hopkins et al. (2021b) to the Voyager, AMS-02, and *Fermi* data.

The second primary class of models are 'self-confinement' (SC) scenarios (Skilling 1975), in which CRs excite Alfvén waves as they stream down their pressure gradients, which dominates the generation of gyro-resonant fluctuations in **B** which subsequently scatter CRs. The CR scattering is determined by the balance of the growth and damping of these gyro-resonant Alfvén waves and so model variants within this class are sensitive to the choice of Alfvén speed, assumptions regarding the wave damping and growth terms, and uncertainties in the turbulent dissipation time-scales. The key scaling here for ultra-relativistic CRs is $\nu \propto (\frac{e_{\rm CR}}{e_{\rm B}})(\frac{v_{\rm A}\,c}{\ell_{\rm CR} r_{\rm L} \Gamma})$ in terms of the magnetic and CR energy densities $e_{\rm B}$, $e_{\rm CR}$; Alfvén speed $v_{\rm A}$; gradient scale length $\ell_{\rm CR}$; gyro radius $r_{\rm L}$; and plasma damping terms Γ. These are again renormalized in Hopkins et al. (2021b) to fit the aforementioned ∼1–10 GeV observations.

The subset of model variants from Hopkins et al. (2021b) explored here were shown to reasonably reproduce observables of γ-ray emission, effective isotropic diffusivities, and CR energy densities at the 'Solar circle', though we will also describe results for simulations which were not consistent with the above constraints to illustrate qualitative differences tying the physics of the model class to the synchrotron properties.

We also compare these model variants to a FIRE-2 simulation that uses a spatially and temporally constant scattering rate (hereafter called the'constant diffusivity' or CD run) presented in Hopkins et al. (2020), and whose magnetic field properties were detailed extensively in Ponnada et al. (2022). This run's constant parallel diffusivity is $\kappa_\parallel = 3 \times 10^{29}$ cm^2 s^{-1}, which was chosen to be consistent with the aforementioned constraints (Chan et al. 2019).

To generate our synchrotron predictions, we follow the procedure outlined in Ponnada et al. (2024), with the caveat that as these are 'single-bin' simulations, we assume a constant CR electron (CRe) spectral shape of Bisschoff, Potgieter & Aslam (2019) and scale the spectrum by the ratio of each gas cell's self-consistently evolved $e_{\rm CR}$ to the local ISM value. This is akin to assuming a constant proton-to-electron ratio as well as a constant spectral shape. Since Bisschoff et al. (2019) provide an empirical spectrum, we are assuming that these models have been tuned to give the right spectral slope according to constraints at MW Solar circle, though see Kempski & Quataert (2022) and Hopkins et al. (2022) for why this may not be physically possible in practice.

Subsequently, the following analysis cannot capture the effects of potential variation in spectral shape and proton-to-electron ratios owing to varying CRe loss terms in gas of different phases and ionization states, nor variation owing to the varied CR transport models and their coupling to gas properties. However, this provides a first look at how the emission properties differ to first order owing to dynamical differences and corresponding effects on phase structure and gas properties owing to CR transport effects, notwithstanding the caveats mentioned above.

3 SYNCHROTRON EMISSION AND THE PHYSICS OF COSMIC RAY TRANSPORT

We examine the synchrotron emission and magnetic field structure from two representative model variants in the ET and SC model classes in Fig. 1 and characterize key differences in the properties of the gas giving rise to the emission.

[1] https://fire.northwestern.edu/

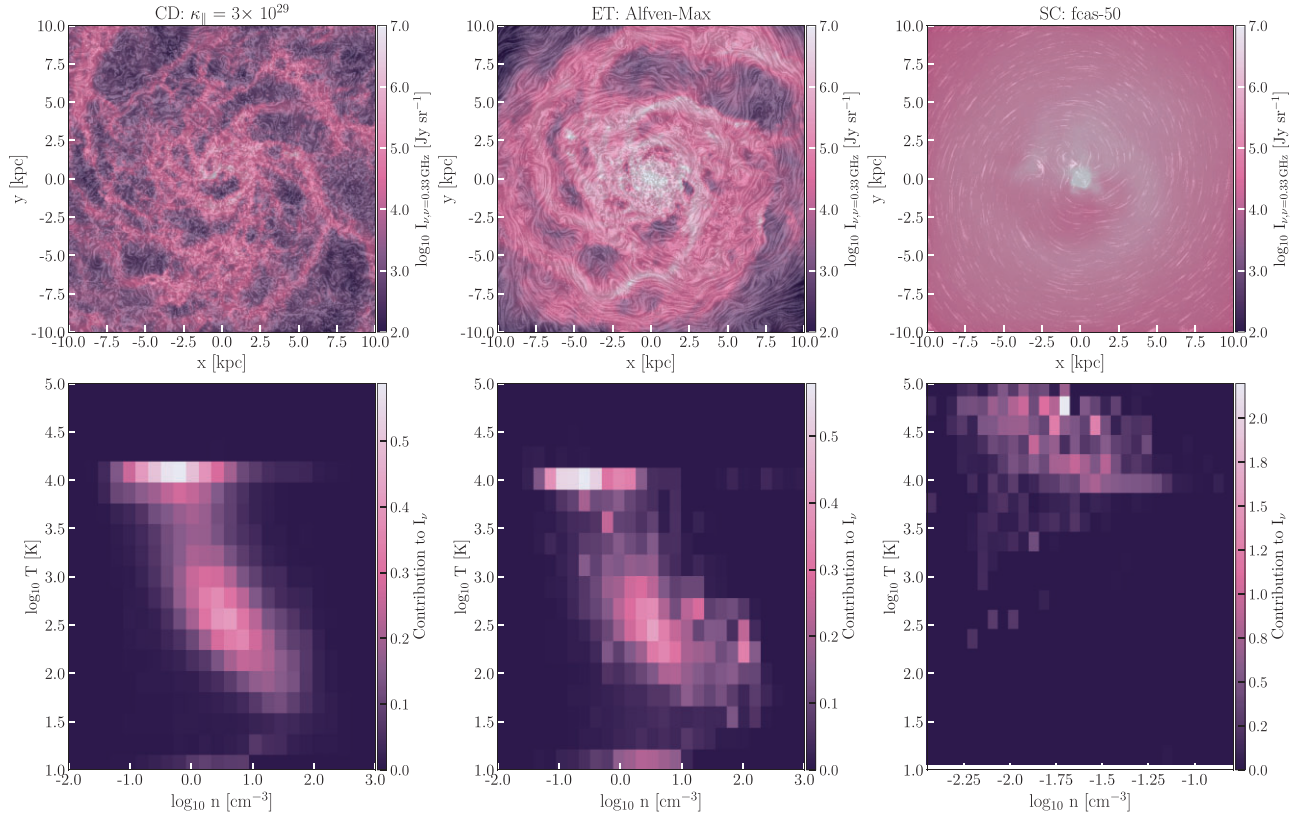

Figure 1. Visualizations of the synchrotron emission at 0.33 GHz and intensity-weighted phase diagrams for FIRE-2 simulations of `m12i` with varied CR transport physics at$z = 0$. Row 1: specific intensity maps with superimposed lines showing the orientation of the mass-averaged components of the magnetic field. A model variant with spatially and temporally constant $\kappa_\parallel = 3 \times 10^{29}$ cm s^{-1} is shown on the left, a variant within the ET class of models ('Alfvén-Max') is shown in the middle, and a SC model ('fcas-50') on the right. CD and ET models generally exhibit more turbulent structure in the magnetic fields, weaker emission, and more variation in brightness contrast to highly ordered **B** and brighter and smoother emission in the SC models. Row 2: intensity-weighted histograms for $2 < R/\mathrm{kpc} < 10$ and $|z| < 3$ kpc for the CD, ET and SC runs above. We exclude the central 2 kpc in order to characterize the extended emission properties rather than the bright central cores. In SC models, the synchrotron emission primarily arises from the WIM/WNM compared to the CNM/WNM dominated scenario in the CD and ET runs.

There appears to be a dichotomy, on average, in the physical morphologies of the galaxies in the two model classes. ET runs exhibit more typical spiral structure and SC runs have a more central bulge-dominated, lenticular-like appearance. The SC runs tend to show brighter, smoother, and more extended emission and have more ordered magnetic field structure relative to the ET runs; ET runs look qualitatively similar to the constant diffusivity run, with brighter emission coincident with the spiral arms and neutral gas structures in the galactic centre. The physical differences underpinning the visual differences between the ET and SC runs become clear in the intensity weighted histograms (Fig. 1, bottom panels). Fig. 1 shows that the extended emission in the ET runs is primarily arising from the denser cool and warm neutral gas, while the SC runs have emission mostly arising from warmer and more diffuse gas.

In Fig. 2, we examine these differences more quantitatively with radial profiles of the forward-modelled synchrotron emission for CR physics model variants simulated in Hopkins et al. (2021b) that met their reasonable observational γ-ray and $e_{\rm CR}$ constraints. We see significant variation in the profiles depending on CR transport physics. We see a separation between the ET and SC model variants: SC runs typically exhibit brighter emission averaged at a given radius by a factor of ∼3–10 relative to ET runs, despite brighter clumped peaks in the spiral arms of ET runs. The SC runs also exhibit smoother emission that falls off more gradually with radius relative to ET and constant diffusivity runs. We stress that the correlation is *not* one-to-one; we can see many earlier (higher redshift) snapshots where the SC models look more like ET. And some simulations with very low constant diffusivity (2 dex lower than observationally allowed) look similar to the SC runs. We discuss this below.

While the radial profiles for the SC runs appear to be qualitatively more similar to a couple of the known observational profiles in that they exhibit a shallower fall-off with radius (Basu & Roy 2013; Beck 2015), the apparent morphological features of the galaxies look markedly different. We defer a comprehensive observational comparison to future work using spectrally resolved cosmological runs. The variation in the synchrotron profiles between classes of CR transport models indicate the potential for the comparison of larger samples of spatially resolved synchrotron images to model predictions to constrain deeply uncertain CR transport physics.

The shape, normalization, and scatter in the profiles is a function of the phase of the ISM dominating the galaxy. The smoothness of the SC profiles is induced by the emission arising mostly from the warm neutral/warm ionized media (WNM/WIM), while on the other hand, the synchrotron intensity profiles of the ET and CD runs are dominated by emission coming from the WNM and denser cold neutral medium (CNM). This key physical difference appears to be driven by differences in the CR transport physics between the SC and ET models, as we will describe in the next section.

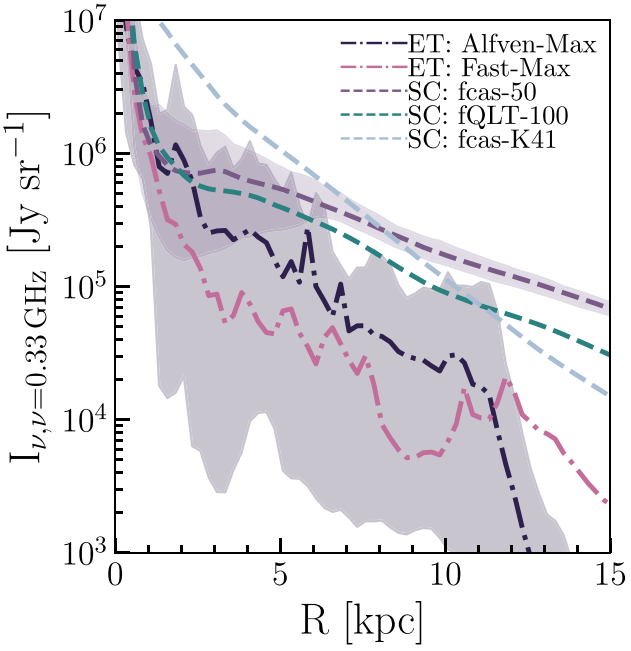

Figure 2. Azimuthally averaged, face-on radial profiles of synchrotron specific intensity for FIRE-2 simulations of `m12i` with varied CR transport physics at$z = 0$. Lines show simulations with ET (dotted–dashed) and SC (dashed) model variants of CR transport. Shaded regions show the 5 per cent–95 per cent range at a given radial bin. Our predictions show significant differences in the shape and normalization of the synchrotron emission profiles, with pathologically different behaviours exhibited between model classes. SC models tend to show brighter, smoother, and more extended profiles in comparison to ET and CD models. The difference in the profiles arises qualitative differences in the phase structure, magnetic field properties, and gas distribution modulated by a CR-physics-driven hysteresis.

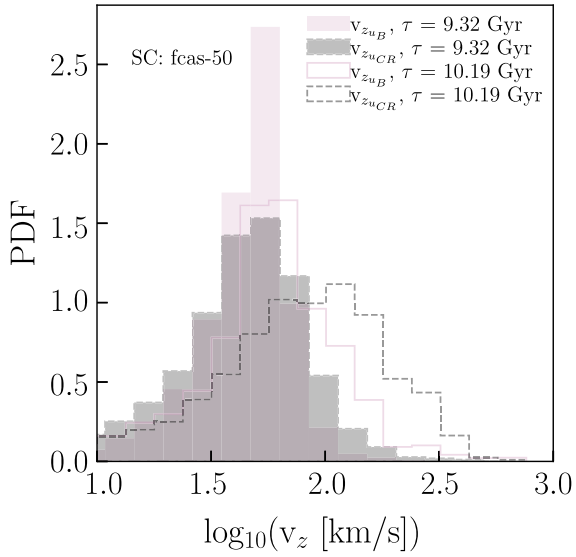

Figure 3. PDFs of the gas velocity $\log_{10}(|v_z|)$ weighted by u_B (dashed) and e_{CR} (solid) at two snapshots 820 Myr apart (filled and unfilled) for $R <$ 14 kpc at heights from the mid-plane of 0.5–3 kpc for an SC run ('fcas-50'). Runs with SC model variants for CR transport appear to be more likely to undergo extreme feedback scenarios in which a build-up of e_{CR} runs away until expelling highly magnetized and e_{CR}-loaded winds from the galaxy. These winds carry away cool, neutral gas, and transform the phase structure and corresponding observable properties of the synchrotron emission.

3.1 A cosmic ray physics-driven hysteresis

The striking differences between the observables and properties of the CD, ET, and SC models boil down to some crucial differences in the physics of CR transport. One of the main features of SC models is the (general) scaling of the scattering rate (see Section 2) as $\nu \propto e_{CR}$, that is, the effective/emergent diffusion coefficient is inversely proportional to e_{CR} ($\kappa_\parallel \propto e_{CR}^{-1}$ in SC model variants, which is the defining characteristic of these types of models; for exact scalings of the models variants considered, see Hopkins et al. 2021b). This scaling is true when the linear damping term dominates the gyro-resonant Alfv´en waves, and the CR flux is in approximate local steady state. This inverse scaling of the diffusion coefficient with the CR energy density can lead to scenarios in which regions of high e_{CR} are prone to more efficient trapping of CRs. This trapping of CRs then leads to the limit of increasing e_{CR}, therefore increasing ν and so on until $\nu \to \infty$, and the CRs are trapped to move strictly with Alfvén wave packets in the gas. This means a large CR pressure has built up and been 'trapped' in the dense ISM gas. This build-up of CR pressure eventually blows apart ISM gas, and thus the galaxy is largely filled with warm/hot and diffuse phases, with dense, magnetized, CR-laden gas spread via these outflows into a much larger, smoother distribution. In contrast, regions of high e_{CR} in ET runs would rapidly diffuse/escape, and due to high e_{CR} compressive modes can be effectively damped, even further 'de-confining' CRs locally.

This difference in the behaviour of CRs especially at high e_{CR} seems to underpin a CR physics-driven hysteresis between the SC model variants and the rest. In SC runs, at $z = 0$ we typically see a warmer and more diffuse phase structure, lower gas surface densities outside $R \sim 4$ kpc, stronger and more ordered **B** at a given n_{gas} and at a given radius, and a steeper e_{CR}–n_{gas} relation. These differences primarily appear to arise after a non-linear feedback event owing to the SC-runaway in which CRs expel most of the cool and neutral gas outside of $R \sim 4$ kpc. At the earlier snapshots this has not yet occurred; it is of course possible that no runaway occurs, but based on the analysis of the three SC-motivated runs that meet constraints here, as well as six of the SC-motivated runs that failed to meet constraints in (Hopkins et al. 2021b), we conclude that it happens eventually than not, as we do not see *any* SC-motivated runs that do not suffer from this issue.

To see this in more detail, in Fig. 3, we show PDFs of the vertical component of velocity ($|v_z|$) weighted by u_B and e_{CR} for two snapshots ~820 Myr apart of the SC run 'fcas-50' at displacements of 0.5–3 kpc from the disc mid-plane. The later snapshot has clear signatures of a feedback event, with the e_{CR}-weighted velocity PDF shifting to having many gas cells with $|v_z| > 100$ km s^{-1}, and the magnetic energy density-weighted probability distribution function (PDF) shifting similarly, though with lower magnitude. The presence of these e_{CR}-loaded winds corresponds directly with a transition in these SC runs from morphological spirals with relatively similar gas distributions, ISM phase structure, and magnetic field properties to the ET and CD runs.

While we show only the velocity PDFs for 'fcas-50', this general picture of e_{CR}-loaded winds, which drive substantial changes in the galaxy properties and synchrotron observables appears to emerge for the other SC models explored in this paper as well. As further confirmation of this process, we note that we see a similar effect of CR and u_B-loaded winds from 'trapped' CRs in runs not shown here but run in Hopkins et al. (2021b) where they adopted a constant but extremely large scattering rate (very low diffusivity, factors >100

lower than the observationally allowed values). As noted by those authors, those particular runs were strongly ruled out by CR spectra, primary-to-secondary ratios, and γ-ray emission in the Galaxy, hence our not comparing them further here. But, by definition, they produce efficient CR trapping, so it should not be surprising that they can produce a similar 'blowout' event to the SC runs here. This demonstrates a new prediction for variations of CR transport models in the SC regime: if CR transport at 1–10 GeV is dominated by modulation from self-excited, gyro-resonant Alfvén waves, galaxies may be more conducive to 'ejective feedback' scenarios through CR-driven winds.

4 DISCUSSION AND CONCLUSIONS

In this work, we explore the effects of different physically motivated models for the CR scattering rate ν which allow it to vary dynamically as function of local plasma properties, heuristically motivated by SC and ET models, in 'single-bin' simulations (not evolving the full CR spectrum) calibrated to give reasonable mean $\langle\nu\rangle$ at ∼GeV energies in Hopkins et al. (2021b).

Simulated galaxies with SC models of CR transport tend to have brighter, more spatially extended and smoother synchrotron emission than ET and CD models. The brighter emission in the SC models corresponds with a relatively featureless, warm-hot phase-dominated ISM, elevated $\mathbf{B}$–n_{gas} relation, and a more ordered and mean-field dominated $\mathbf{B}$. This apparent hysteresis seems to be CR physics driven, as SC runs have the potential for a runaway at high e_{CR} which leads to CR energy concentrating until cold and dense gas is blown out via e_{CR} and u_B loaded winds, resulting in the stark morphological and physical differences between SC and ET/CD runs.

Already, the sheer lack of detailed cold, neutral phase structure diverges from typical $\sim L_*$ spiral galaxies, which may indicate that SC is not the dominant mode of CR transport in these types of galaxies, though it may operate more so within galaxies with a lenticular-like morphology with a more featureless gas/dust distribution. Despite this, the radial intensity profiles of the SC models are characteristically less steep than those of CD/ET models, and more similar in shape to the small sample of observed radial profiles compared to in Ponnada et al. (2024). This may also indicate that something is missing from ET models, but we have not found a way to hybridize this model class with SC scalings in a way that does not suffer the 'SC runaway' effects. It is easier in principle to reconcile the relative steepness of ET synchrotron emission profiles with physics not directly related to the CR transport scalings through slightly higher gas surface densities or magnetic field strengths. However, this work indicates the potential for differences between CR transport models to be probed in a spatially resolved manner with larger samples with future radio instruments like the DSA-2000 (Hallinan et al. 2019), ngVLA (Murphy et al. 2018), and Square Kilometer Array (Dewdney et al. 2009) and with already existing and future H I 21 cm surveys (Walter et al. 2008).

We emphasize also that the differences seen in the model variations here are highly non-linear, and do not indicate that SC models of CR transport will *always* exhibit these differences relative to ET/CD models. Rather, the predictions made here are for SC transport models which have undergone the 'SC runaway,' and simulations which have not undergone this nonlinear process (like higher redshift snapshots or those not run with the SC transport scalings fully cosmologically) do not exhibit the same characteristic synchrotron properties. And we stress that, as shown in more detail in Hopkins et al. (2021b, 2022), qualitative and order-of-magnitude uncertainties remain in first-principle models for the CR scattering rate ν and indeed *no* first-principle model has been demonstrated to predict the correct CR spectra and primary-to-secondary ratios at ∼MeV–TeV energies (Hopkins et al. 2022).

And although the differences explored here appear to be driven by the CR physics, there are several other interrelated factors that may be important. Notably, the non-linear interplay of our stellar feedback model, the coupling of CR feedback, and the physics of gas cooling altogether influence the corresponding gas properties and are not cleanly separable i.e. these are the predictions of these CR transport models *given* the FIRE-2 feedback and cooling physics and numerics. Changing the feedback and cooling prescriptions might lead to different results for the effect of the CR transport models on the synchrotron emission properties of simulated galaxies. The exact timing and prominence of these 'blowout' events may also potentially depend on the gas resolution, which we will increase in future studies to $\sim 7000\ M_\odot$, though we have checked the same CR transport variants for an intermediate-mass simulated galaxy (`m11f` in Hopkins et al. (2021b), factor of ∼2 lower in halo mass than the simulations presented here) at a higher Lagrangian mass resolution of $12\,000\ M_\odot$ and found similar results. The dynamical interaction of CRs again highlights the need for explicit evolution of CRs in galaxy formation simulations, as tracer particle or post-processing approaches to CR transport, for instance, popular methods like those of GALPROP (Strong & Moskalenko 1998) would by construction fail to capture these important effects.

Future work will include the exploration of more FIRE-3 simulations which vary CR transport and explicitly evolve CR(e) spectra beyond the 'single-bin' simulations explored in this work. These FIRE-3 simulations will allow for the generation of more robust synchrotron predictions (i.e. spectral variation) that may generate new predictions for conducting observational tests of CR transport models. In a similar vein, multiwavelength analysis of varied CR transport models, for example with spatial cross-correlations, may prove fruitful in generating more predictive constraints that can be tested against observations.

ACKNOWLEDGEMENTS

We wish to recognize and acknowledge the past and present Gabrielino–Tongva people and their Indigenous lands upon which this research was conducted. Additionally, we thank the staff at our institutes, without whose endless efforts this work would not be possible during the ongoing pandemic. Support for SP and PFH was provided by NSF Research grants 1911233, 20009234, and 2108318, NSF CAREER grant 1455342, NASA grants 80NSSC18K0562 and HST-AR-15800. GVP acknowledges support by NASA through the NASA Hubble Fellowship grant no. HST-HF2-51444.001-A awarded by the Space Telescope Science Institute, which is operated by the Association of Universities for Research in Astronomy, Incorporated, under NASA contract NAS5-26555. CBH is supported by NSF grant AAG-1911233 and NASA grants HST-AR-15800, HST-AR-16633, and HST-GO-16703. Numerical calculations were run on the Caltech compute cluster 'Wheeler,' allocation AST21010 supported by the NSF and TACC, and NASA HEC SMD-16-7592. The Flatiron Institute is supported by the Simons Foundation. CAFG was supported by NSF through grants AST-2108230 and CAREER award AST-1652522; by NASA through grants 17-ATP17-0067 and 21-ATP21-0036; by STScI through grant HST-GO-16730.016-A; by CXO through grant TM2-23005X; and by the Research Corporation for Science Advancement through a Cottrell Scholar Award. ISB was supported by the DuBridge Postdoctoral Fellowship at Caltech. DK was supported by NSF grant AST2108314. KS acknowledges

support from the Black Hole Initiative at Harvard University, which is funded by grants from the John Templeton Foundation and the Gordon and Betty Moore Foundation. This work was supported by NSF grant AST-2109127.

DATA AVAILABILITY

The data supporting the plots within this article are available on reasonable request to the corresponding author. A public version of the GIZMO code is available at http://www.tapir.caltech.edu/~phopkins/Site/GIZMO.html. FIRE-2 simulations are publicly available (Wetzel et al. 2022) at http://flathub.flatironinstitute.org/fire, though simulations including the physics of MHD and CRs like those analysed in this study are not yet publicly available. Additional data, including initial conditions and derived data products, are available at https://fire.northwestern.edu/data/.

REFERENCES

Armillotta L., Ostriker E. C., Jiang Y.-F., 2022, ApJ, 929, 170
Basu A., Roy S., 2013, MNRAS, 433, 1675
Beck R., 2015, A&A, 578, A93
Bell A. R., 1978, MNRAS, 182, 147
Bisschoff D., Potgieter M. S., Aslam O. P. M., 2019, ApJ, 878, 59
Booth C. M., Agertz O., Kravtsov A. V., Gnedin N. Y., 2013, ApJ, 777, L16
Boulares A., Cox D. P., 1990, ApJ, 365, 544
Buck T., Pfrommer C., Pakmor R., Grand R. J., Springel V., 2020, MNRAS, 497, 1712
Bustard C., Zweibel E. G., D'Onghia E., Gallagher J. S., III, Farber R., 2020, ApJ, 893, 29
Butsky I. S., Quinn T. R., 2018, ApJ, 868, 108
Butsky I. S., Fielding D. B., Hayward C. C., Hummels C. B., Quinn T. R., Werk J. K., 2020, ApJ, 903, 77
Butsky I. S. et al., 2022, ApJ, 935, 69
Butsky I. S., Nakum S., Ponnada S. B., Hummels C. B., Ji S., Hopkins P. F., 2023, MNRAS, 521, 2477
Chan T. K., Kereš D., Hopkins P. F., Quataert E., Su K. Y., Hayward C. C., Faucher-Giguère C. A., 2019, MNRAS, 488, 3716
Chan T. K., Kereš D., Gurvich A. B., Hopkins P., Trapp C., Ji S., Faucher-Giguère C.-A., 2021, MNRAS, 517, 597
Dewdney P. E., Hall P. J., Schilizzi R. T., Lazio T. J. L. W., 2009, IEEE Proc., 97, 1482
Farcy M., Rosdahl J., Dubois Y., Blaizot J., Martin-Alvarez S., 2022, MNRAS, 513, 5000
Girichidis P. et al., 2016, ApJ, 816, L19
Hallinan G. et al., 2019, BAAS, 51, 255
Hopkins P. F., 2016, MNRAS, 462, 576
Hopkins P. F., 2017, MNRAS, 466, 3387
Hopkins P. F., Raives M. J., 2016, MNRAS, 455, 51
Hopkins P. F. et al., 2018, MNRAS, 480, 800
Hopkins P. F. et al., 2020, MNRAS, 492, 3465
Hopkins P. F., Chan T. K., Squire J., Quataert E., Ji S., Kereš D., Faucher-Giguère C.-A., 2021a, MNRAS, 501, 3663
Hopkins P. F., Squire J., Chan T. K., Quataert E., Ji S., Kereš D., Faucher-Giguère C.-A., 2021b, MNRAS, 501, 4184
Hopkins P. F., Squire J., Butsky I. S., Ji S., 2022, MNRAS, 517, 5413
Huang X., Davis S. W., 2022, MNRAS, 511, 5125
Huang X., Jiang Y.-F., Davis S. W., 2022, ApJ, 931, 140
Ji S. et al., 2020, MNRAS, 496, 4221
Jokipii J. R., 1966, ApJ, 146, 480
Kempski P., Quataert E., 2022, MNRAS, 514, 657
Lacki B. C., Thompson T. A., Quataert E., Loeb A., Waxman E., 2011, ApJ, 734, 107
Modak S., Quataert E., Jiang Y.-F., Thompson T. A., 2023, MNRAS, 524, 6374
Murphy E. J. et al., 2018, in Murphy E.ed., ASP Conf. Ser., Vol. 517, Science with a Next Generation Very Large Array. Astron. Soc. Pac., San Francisco, p. 3
Owen E. R., Wu K., Inoue Y., Yang H. Y. K., Mitchell A. M. W., 2023, Galaxies, 11, 86
Pakmor R., Pfrommer C., Simpson C. M., Springel V., 2016, ApJL, 824, L30
Ponnada S. B. et al., 2022, MNRAS, 516, 4417
Ponnada S. B. et al., 2024, MNRAS, 527, 11707
Quataert E., Thompson T. A., Jiang Y.-F., 2022, MNRAS, 510, 1184
Ruszkowski M., Pfrommer C., 2023, A&AR, 31, 4
Salem M., Bryan G. L., 2014, MNRAS, 437, 3312
Salem M., Bryan G. L., Corlies L., 2016, MNRAS, 456, 582
Simpson C. M., Pakmor R., Marinacci F., Pfrommer C., Springel V., Glover S. C. O., Clark P. C., Smith R. J., 2016, ApJ, 827, L29
Skilling J., 1975, MNRAS, 172, 557
Strong A. W., Moskalenko I. V., 1998, ApJ, 509, 212
Tang Q.-W., Wang X.-Y., Tam P.-H. T., 2014, ApJ, 794, 26
Thomas T., Pfrommer C., Pakmor R., 2023, MNRAS, 521, 3023
Tsung T. H. N., Oh S. P., Bustard C., 2023, MNRAS, 526, 3301
Walter F., Brinks E., de Blok W. J. G., Bigiel F., Kennicutt Robert C. J., Thornley M. D., Leroy A., 2008, AJ, 136, 2563
Wetzel A. et al., 2023, ApJS, 265, 44

This paper has been typeset from a TEX/LATEX file prepared by the author.